JACS
JOURNAL OF THE AMERICAN CHEMICAL SOCIETY
pubs.acs.org/JACS

Article

Stabilization of the $[C_2N_5]^{7-}$ Anion in Recoverable High-Pressure $Eu_4Fe_{0.864(6)}(C_2N_5)_2$ Pyronitridocarbonate

Fariia Iasmin Akbar,* Nityasagar Jena,* Christian Tobeck, Pascal L. Jurzick, Niko T. Flosbach, Valerio Cerantola, Elena Bykova, Lukas Brüning, Andrey Aslandukov, Dominik Spahr, Valentin Kovalev, Gaston Garbarino, Anna Pakhomova, Georgios Aprilis, Nico Giordano, Leonid Dubrovinsky, Mathias S. Wickleder, Uwe Ruschewitz, Igor A. Abrikosov, and Maxim Bykov*

Cite This: J. Am. Chem. Soc. 2026, 148, 11915−11924

Read Online

ACCESS | Metrics & More | Article Recommendations | Supporting Information

ABSTRACT: Synthesis at extreme conditions enables access to nitrogen-rich carbon−nitrogen anions that cannot be obtained at ambient conditions. Here, through a direct reaction between $Eu(N_3)_2$ and EuC_2 with Fe in a laser-heated diamond anvil cell (DAC) at 50(3) GPa, we synthesized the first inorganic hydrogen-free pyronitridocarbonate, $Eu_4Fe_x(C_2N_5)_2$, $x = 0.864(6)$, featuring novel highly charged $[C_2N_5]^{7-}$ anions, along with the first stoichiometric oxygen-free rare-earth metal guanidinate $Eu_5(CN_3)_3$. The crystal structures of both compounds were determined via synchrotron single-crystal X-ray diffraction (SCXRD) and fully corroborated by density functional theory (DFT) calculations. $Eu_4Fe_x(C_2N_5)_2$ was found to be recoverable at pressures close to ambient. Keeping the sample at ambient conditions for 1 day leads to splitting of half of the $[C_2N_5]^{7-}$ units in $Eu_4Fe_x(C_2N_5)_2$ into the guanidinate $[CN_3]^{5-}$ and carbodiimide $[CN_2]^{2-}$ anions. The statistical analysis of the multigrain SCXRD data and DFT-based electronic structure analysis well defined the chemical nature of the bonding in $[C_2N_5]^{7-}$ and $[CN_3]^{5-}$ anions. This study provides a clear synthetic pathway to a new class of inorganic nitridocarbonates.

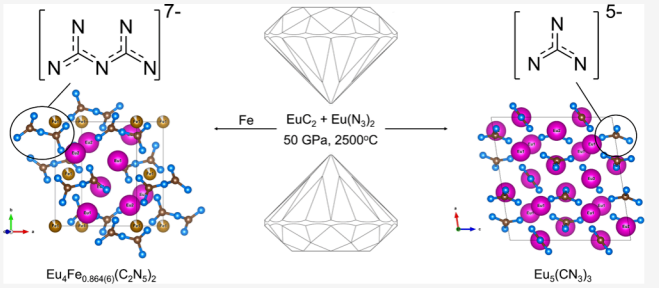

INTRODUCTION

Synthesis and stabilization of compounds containing complex nitridocarbonate anions is an emerging topic in high-pressure chemistry, offering access to previously unknown bonding motifs and highly charged carbon−nitrogen species. Carbon−nitrogen anions occur in important classes of inorganic solids and include widely studied cyanides $[CN]^-$[1] and carbodiimides $[CN_2]^{2-}$,[2,3] as well as less common acetonitriletriides $[C_2N]^{3-}$,[4,5] dicyanamides $[N(CN)_2]^-$,[6] tricyanidomethanides $[C(CN)_3]^-$,[7] tetracyanoethylene radicals $[C_2(CN)_4]^{\bullet-}$,[8] pentacyanoethanides $[C_2(CN)_5]^-$,[9] pentacyanopropenides $[NCC\{C(CN)_2\}_2]^-$,[10,11] guanidinates $[CN_3]^{5-}$,[12] tricyanidomelaminates $[C_6N_9]^{3-}$,[13] melonates $[C_6N_7(NCN)_3]^{3-}$,[14] cyanopolyynides $[C_{2n+1}N]^-$ (n = 0, 1, 2),[15] cyano adduct anions of fullerenes $[C_{60}(CN)_n]^-$ (n = 1, 3, 5),[16] $[C_{60}(CN)_n]^{2-}$ (n = 2, 4, 6),[17] $[C_{70}(CN)_n]^-$ (n = 1, 2, 3), and $[C_{70}(CN)_n]^{2-}$ (n = 2, 4, 6).[18] Ternary M−C−N compounds featuring nitrogen−nitrogen bonds are represented by the derivatives of tetrazole, e.g., 5-azidotetrazolate $[CN_7]^-$,[19] 5,5′-azotetrazolate $[N_2(CN_4)_2]^{2-}$,[20,21] and 4,5-bis(tetrazol-5-*yl*)-2H-1,2,3-triazolate $[C_2N_3(CN_4)_2]^{3-}$.[22]

Despite this structural diversity, most C−N anions remain nitrogen-poor. High-pressure synthesis is effective way to stabilize nitrogen-rich species, as was shown on the examples of various polynitrides.[23−30] Recent high-pressure reactions in multicomponent C−N systems yielded compounds featuring guanidinate $[CN_3]^{5-}$,[31,32] melaminate $[C_3N_6]^{6-}$,[33,34] as well as the poly-*N*-(1,3,5-triazin-2-*yl*)-guanidine anions in $Bi_7C_{10}N_{18}(N_{3(1-x)}O_{3x})$.[35] Syntheses at megabar pressure revealed the formation of polynitridocarbonates formed by anionic three-dimensional framework consisting of CN_4 tetrahedra connected via di- or oligo-nitrogen linkers.[36]

Despite recent discoveries in ternary C−N-containing compounds, many potential forms of C−N anions remain unknown. A similar tendency to form a wide variety of species composed of two light elements has been identified in high-pressure carbonates, where pressure stabilizes pyrocarbonates containing $[C_2O_5]^{2-}$ anions.[37−42] We hypothesize that by analogy with a series of carbonate-pyrocarbonate species, the elusive pyronitridocarbonate anion $[C_2N_5]^{7-}$ may also exist

Received: December 5, 2025
Revised: January 13, 2026
Accepted: January 27, 2026
Published: March 4, 2026

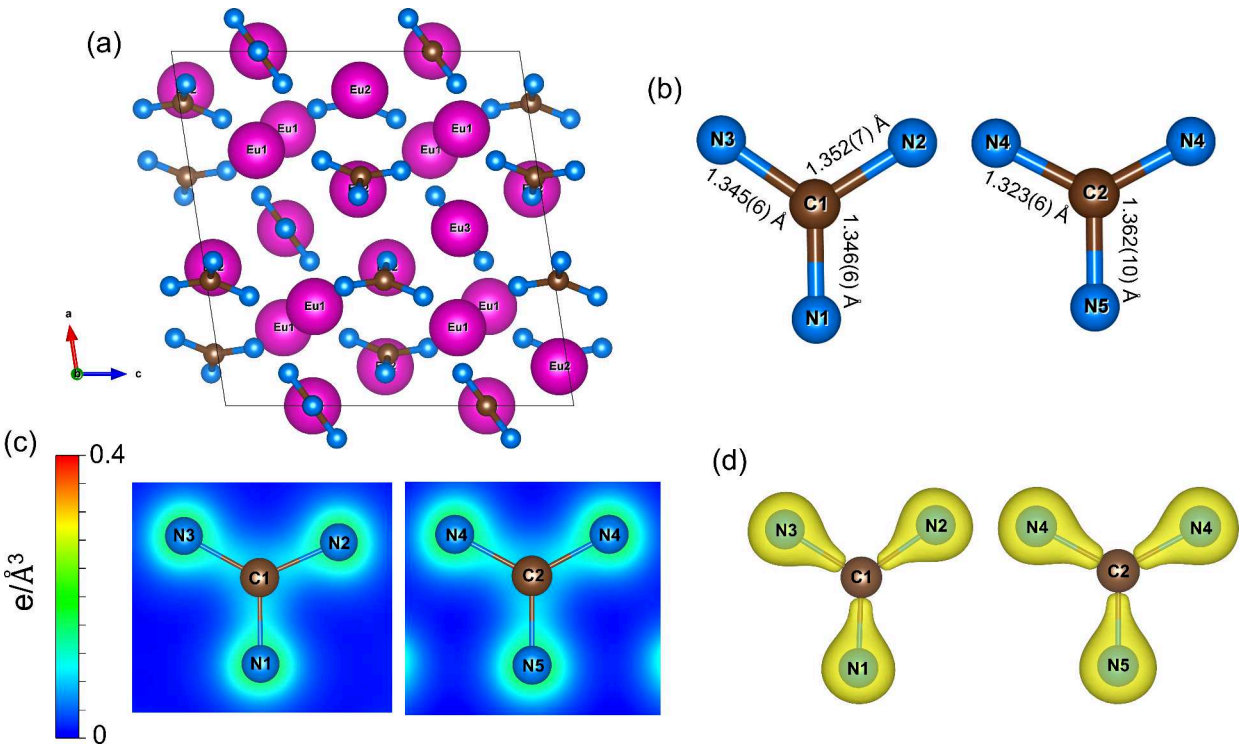

Figure 1. Crystal structure of europium guanidinate $Eu_5(CN_3)_3$ at 50(3) GPa. All Eu atoms are purple, C atoms are brown, and N atoms are blue; gray thin lines outline the unit cell. (a) The unit cell in projection along the *b* axis. (b) A view of the $[CN_3]^{5-}$ units. (c) Charge density distribution in plains containing the $[CN_3]^{5-}$ unit atoms. (d) Charge density isosurfaces of the guanidinate anions (with an isosurface level of 0.3).

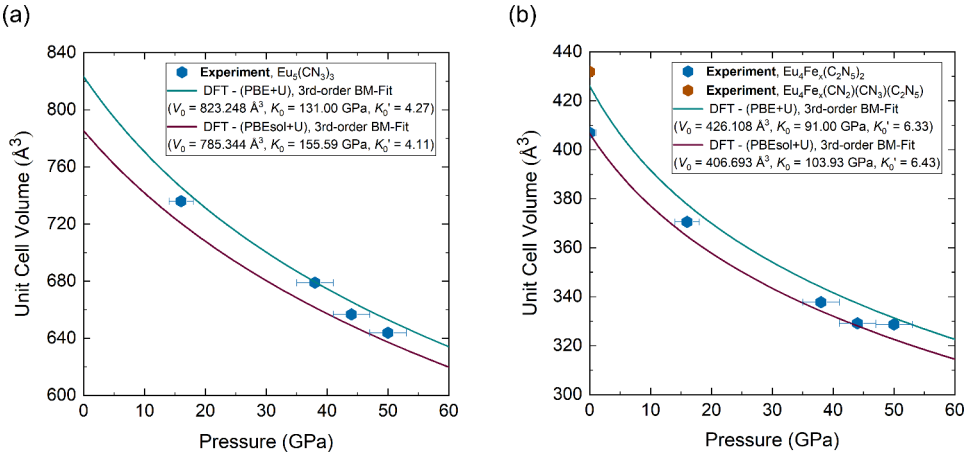

Figure 2. (a) The pressure dependence of the unit cell volume of $Eu_5(CN_3)_3$ over a pressure range of 0−60 GPa, calculated using both PBE+*U* and PBEsol+*U* functionals within the DFT+*U* framework, compared with the experimental data. Solid lines correspond to the third-order Birch−Murnaghan Equation of State (BM3 EoS) based on DFT calculations. (b) The pressure dependence of the unit cell volume of $Eu_4Fe(C_2N_5)_2$. The experimental data at ambient conditions for the $Eu_4Fe(CN_2)(CN_3)(C_2N_5)$ is marked by different color (brown).

and be accessible in a high-pressure synthesis. The biggest challenge is to stabilize a relatively high odd-number charge in a rather small anion. Highly charged anions are typically found either in extended polyanionic frameworks (e.g., in $Bi_7C_{10}N_{18}(N_{3(1-x)}O_{3x})$,[35] $LaCN_3$ and $CeCN_5$[36]) or within large, isolated clusters ($[P_3N_9]^{12-}$ in $Li_{12}P_3N_9$, $[P_4N_{10}]^{10-}$ in α-/β-$Li_{10}P_4N_{10}$, and $[B_3P_3N_{13}]^{15-}$ in $Li_{47}B_3P_{14}N_{42}$).[43] Small highly charged isolated anions are rare. Among examples are the ethanide anions $[C_2]^{6-}$ in Dy_3C_2.[44,45]

In this work, we present the synthesis of the first inorganic hydrogen-free pyronitridocarbonate $Eu_4Fe_{0.864(6)}(C_2N_5)_2$ featuring $[C_2N_5]^{7-}$ anions—fully deprotonated derivatives of biguanide $C_2N_5H_7$.[46] Under similar conditions we also obtained the first stoichiometric oxygen-free rare-earth element nitridocarbonate, $Eu_5(CN_3)_3$.

RESULTS AND DISCUSSION

We employed a new high-pressure synthetic strategy to access ternary and quaternary nitridocarbonates by laser-heating a mixture of europium azide $Eu(N_3)_2$ and europium carbide EuC_2 with a minor amount of iron in a DAC. Products of chemical reaction performed at 50(3) GPa and a temperature of 2800(200) K were identified by means of SCXRD at ESRF (ID15b, ID27) and DESY (P02.2) (see section Methods in the

https://doi.org/10.1021/jacs.5c21756
J. Am. Chem. Soc. 2026, 148, 11915−11924

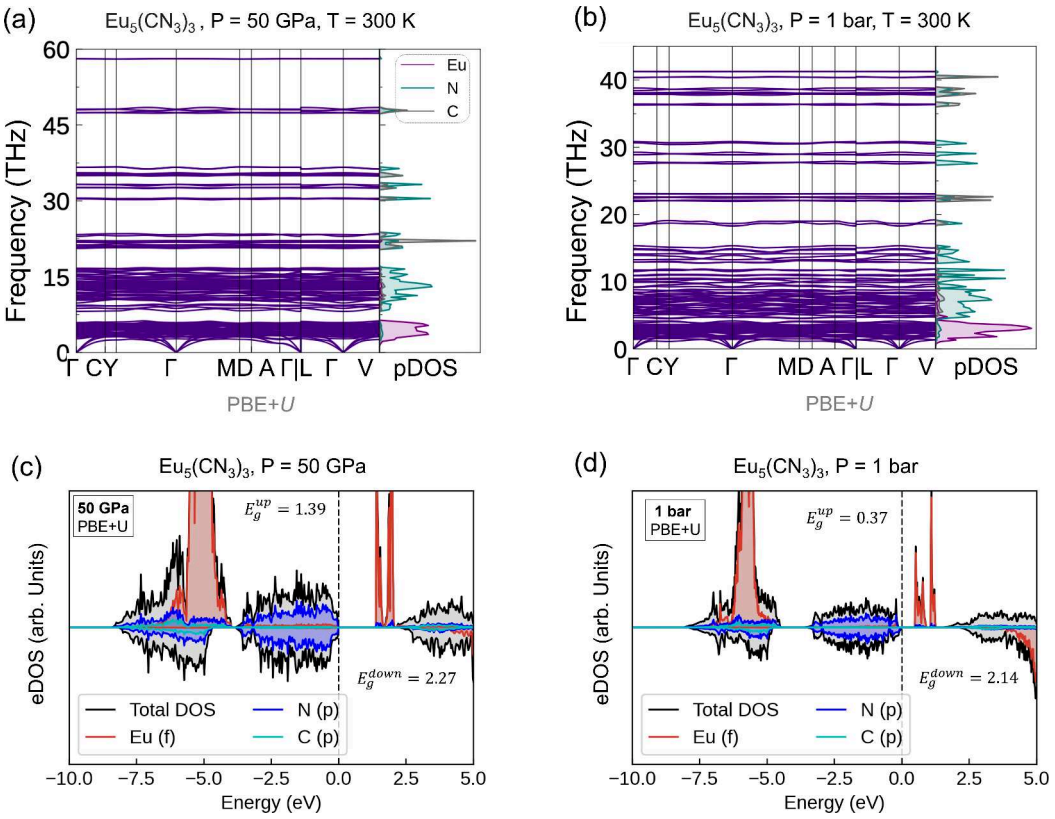

Figure 3. (a)−(b) Finite temperature phonon dispersion relations and the phonon density of states (pDOS) for $Eu_5(CN_3)_3$ at 50 GPa, and 1 bar, respectively, calculated using the sTDEP methods at T = 300 K. (c)−(d) Spin-resolved electronic density of states (eDOS) for $Eu_5(CN_3)_3$ at 50 GPa and 1 bar, respectively, calculated using PBE+U functional.

Supporting Information). The multigrain diffraction data analysis revealed the formation of several novel compounds in the laser-heated area. Full experimental details are provided in Tables S1−S6 and Figures S1−S4 of the Supporting Information. All supplemental results of the theoretical calculations are given in Tables S7−S10, Figures S5−S15, and Discussion S1. In the following sections, we describe the crystal structures and physical properties of two main products: Europium(III) nitridocarbonate $Eu_5(CN_3)_3$ and Europium-(III)−Iron(II)-pyronitridocarbonate $Eu_4Fe_{0.864(6)}(C_2N_5)_2$.

Europium Nitridocarbonate $Eu_5(CN_3)_3$

Europium guanidinate $Eu_5(CN_3)_3$ crystallizes in the monoclinic space group $C2/c$ (Figure 1, Table S2) and contains three crystallographically unique Eu atoms (Eu1 and Eu2 occupying the 8f Wyckoff site, and Eu3 on the 4e site). The structure features two symmetry-independent guanidinate anions $[CN_3]^{5-}$ with C−N distances varying in the range of ∼1.32−1.36 Å (Figure 1b), consistent with those reported for $SbCN_3$,[31] $Ln_3O_2(CN_3)$ (Ln = La, Eu, Gd, Tb, Ho, Yb),[32] $Sr_4(Sr_6N)_2[In_4][CN_3]_4$, and $(Sr_9N_{1.33(8)})(SrIn_3)[CN_3]$,[12] supporting the formal C−N bond order of 1.33. Europium atoms are coordinated by 9 or 10 nitrogen atoms, forming a distorted monocapped tetragonal antiprism (Eu1), a *cis*-bicapped cube (Eu2), and a tricapped trigonal prism (Eu3) (Figure S2a). $Eu_5(CN_3)_3$ remains detectable via synchrotron XRD down to 16(2) GPa during decompression (Table S3).

The experimental crystal structure of $Eu_5(CN_3)_3$ was fully optimized at 50 GPa within the GGA+U framework using both the PBE+U and PBEsol+U functionals. The optimized lattice parameters at 50 GPa exhibit excellent agreement with experimental values obtained from SCXRD data with a deviation of less than 2% (Table S8).

A BM3 EoS was used to describe volume−pressure dependence obtained from DFT calculations in the range of 0−60 GPa, yielding equilibrium unit cell volumes of 823 Å^3 and 785 Å^3 using PBE+U and PBEsol+U functionals, respectively, with an estimated bulk modulus K_0 in the range of 130−155 GPa (Figure 2a). Lattice parameters of $Eu_5(CN_3)_3$ increase monotonically upon pressure release over the entire pressure range without any sign of lattice distortions (Figure S5a). Phonon dispersion relations calculated using the harmonic approximation (Figure S6) indicate dynamical instabilities in $Eu_5(CN_3)_3$ both at the synthesis pressure and at 1 bar, attributed to C−N bond asymmetry in the $[CN_3]^{5-}$ units. This instability is lifted by using finite-temperature phonon dispersion calculations at T = 300 K via the sTDEP method (Figure 3a, b).

Within the PBE+U calculations, at 50 GPa, $Eu_5(CN_3)_3$ is an insulator with an energy gap between the occupied N 2p-states and unoccupied highly localized Eu 4f states of 1.39 eV for the spin-up channel and 2.27 eV for the spin-down channel (Figure 3c). Comparable bandgap values were obtained using the PBEsol+U functional (Table S8, Figures S7a and S8b). $Eu_5(CN_3)_3$ remains insulating over the entire pressure range from 50 GPa to 1 bar (Figure 3c, d).

The occupied Eu 4f states lie at ∼6 eV below the Fermi energy, and nitrogen 2p orbitals dominate the valence band edge. The bandgap of $Eu_5(CN_3)_3$ decreases monotonically upon decompression with an increasing discrepancy between PBE+U and PBEsol+U bandgap energy values (Figure S7a). Each europium atom in $Eu_5(CN_3)_3$ carries a calculated

https://doi.org/10.1021/jacs.5c21756
J. Am. Chem. Soc. 2026, 148, 11915−11924

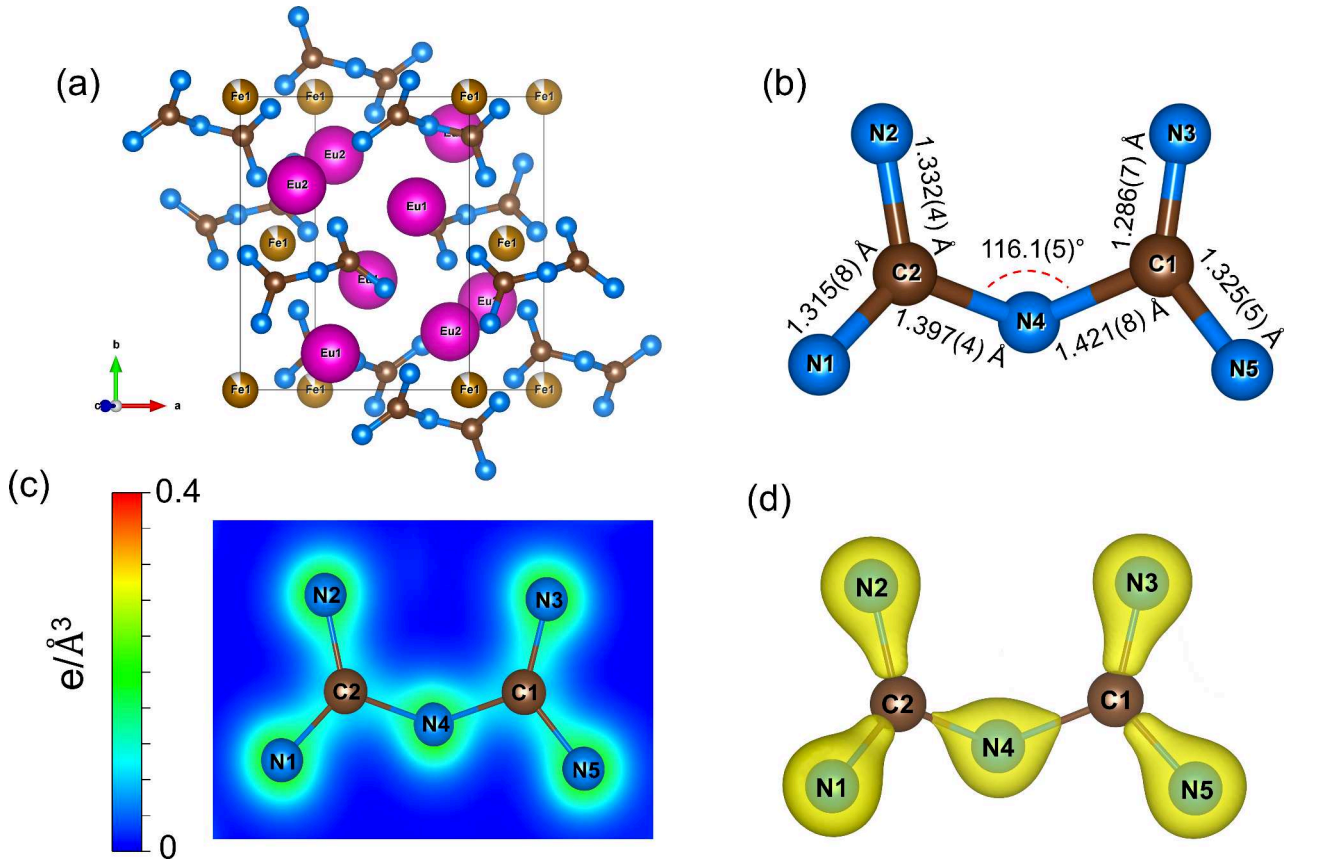

Figure 4. Crystal structure of europium pyronitridocarbonate $Eu_4Fe_x(C_2N_5)_2$ at 50(3) GPa. Eu atoms are purple, Fe atoms are yellow, C atoms are brown, and N atoms are blue; gray thin lines outline the unit cell. (a) A general view of the crystal structure of $Eu_4Fe_x(C_2N_5)_2$. (b) A pyronitridocarbonate anion geometry. (c) Charge density distribution in plains containing the $[C_2N_5]^{7-}$ unit atoms. (d) Charge density isosurface of the pyronitridocarbonate anion (with an isosurface level of 0.3).

magnetic moment of 6 μ_B, with unoccupied localized 4*f* states near the conduction band edge comprising one *f*-electron from each europium atom.

Although the finite-temperature (T = 300 K) phonon dispersion relation calculated for $Eu_5(CN_3)_3$ at ambient pressure shows the lattice dynamic stability of the compound (Figure 3b), it was not observed in our SCXRD experiments below a pressure of 16 GPa (Figure 2a).

Europium–Iron Pyronitridocarbonate $Eu_4Fe_x(C_2N_5)_2$

Europium–iron pyronitridocarbonate, $Eu_4Fe_x(C_2N_5)_2$, x = 0.864(6) (space group $P2_1/c$) (Table S4), contains an unprecedented pyronitridocarbonate $[C_2N_5]^{7-}$ anion (Figures 4 and S3), representing the fully deprotonated form of biguanide $C_2N_5H_7$.[46] Europium, iron, nitrogen, and carbon atoms in $Eu_4Fe_x(C_2N_5)_2$ occupy the following Wyckoff sites: 4*e* (Eu1, Eu2, N1–N5, C1, and C2) and 2*a* (Fe1) (Table S4). Two symmetry-independent Eu atoms, Eu1 and Eu2, are coordinated by 10 and 11 nitrogen atoms, respectively, forming a distorted bicapped tetragonal antiprism and a fully capped trigonal prism. Fe1 atoms feature octahedral coordination (Figure S2b).

The C–N distances in the $[C_2N_5]^{7-}$ units of $Eu_4Fe_x(C_2N_5)_2$, determined at 50(3) GPa, are equal to ~1.40–1.42 Å for bridging nitrogen atoms and ~1.29–1.33 Å for the terminal nitrogen atoms (Figure 4b). Both distance ranges indicate an intermediate state between a single C–N bond (~1.47 Å[47]) and a bond of order 1.5, as observed in pyridine (d_{C-N} ~ 1.34 Å[48,49]). Moreover, bond orders derived from the resonance forms of the biguanide molecule $C_2N_5H_7$[46] are consistent with the C–N distances in the $[C_2N_5]^{7-}$ anions: 1.25 for the bridging atom and 1.375 for the terminal ones. The charge density distribution clearly shows the difference between the bridging and terminal C–N bonds in $[C_2N_5]^{7-}$ (Figure 4c, d), specifically, the peripheral bonds show a more pronounced electron density (Figure 4c, d). The geometry of the observed nonplanar $[C_2N_5]^{7-}$ anions (Figures 4b and S3) can be compared to those in pyrocarbonates, possessing a wide variety of anion geometries.[37−42]

The partial occupancy x = 0.864(6) of Fe in $Eu_4Fe_x(C_2N_5)_2$, along with the interatomic C–N distances, was determined through the statistical analysis of 26 individual structure refinements (as described in the Methods section). The Mössbauer spectrum of $Eu_4Fe_x(C_2N_5)_2$ at 50(3) GPa represents a singlet component with a center shift of 0.26 mm/s (Figure S4), in agreement with a low-spin state of Fe^{2+} in an octahedral coordination.[50,51] The low signal intensity is attributed to the fact that the sample was prepared with naturally occurring iron rather than ^{57}Fe-enriched iron, which is typically used in high-pressure experiments exploiting Mössbauer spectroscopy as an analytical technique. The deviation from 100% Fe site occupancy requires the presence of a fraction of Fe^{III} for the charge balance (e.g., $Eu_3Fe^{II}_{0.592}Fe^{III}_{0.272}(C_2N_5)_2$). The Fe^{III} component, regardless of its spin state, may lie below the detection limit of Mössbauer spectroscopy due to the low signal-to-noise ratio and overlap with the signal from the beamline optics and is therefore not

https://doi.org/10.1021/jacs.5c21756
J. Am. Chem. Soc. 2026, 148, 11915−11924

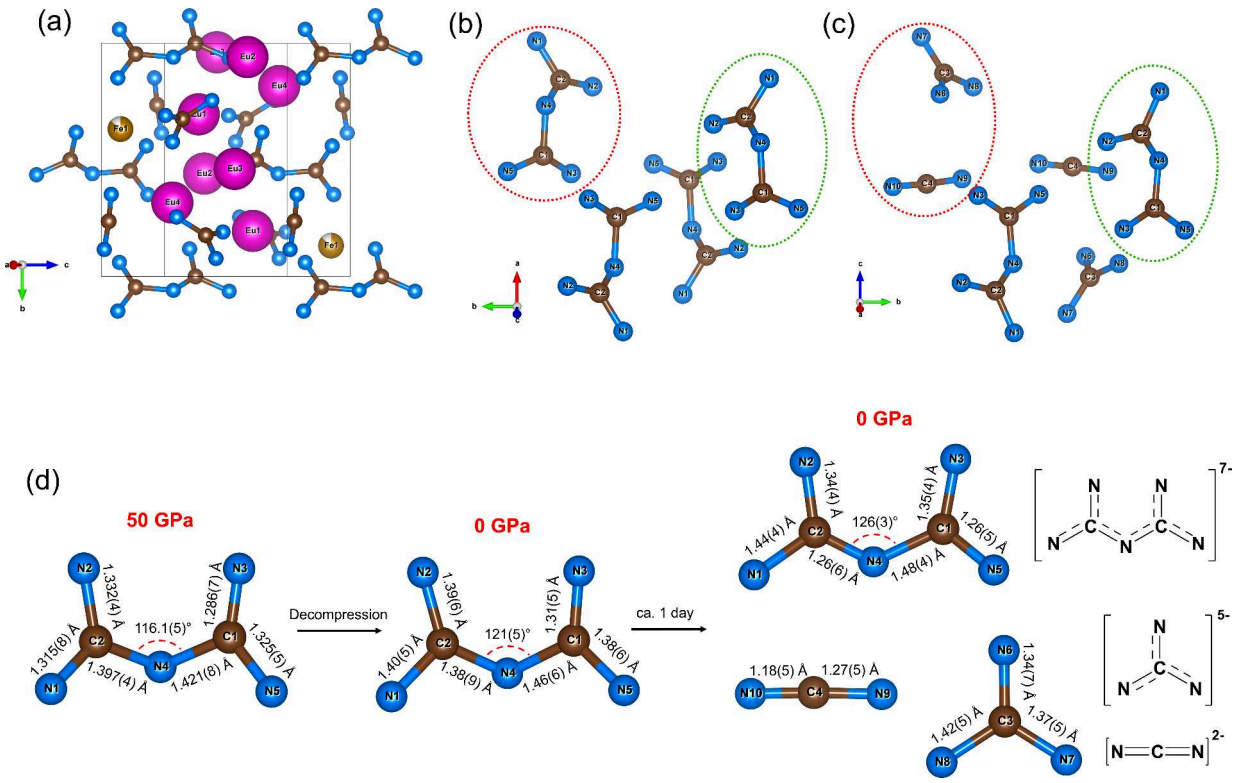

Figure 5. Crystal structure of the europium pyronitridocarbonate after chemical transformation to $Eu_4Fe_x(CN_2)(CN_3)(C_2N_5)$ under ambient conditions. Eu atoms are purple, Fe atoms are yellow, C atoms are brown, and N atoms are blue; gray thin lines outline the unit cell. (a) A general view of the crystal structure of $Eu_4Fe_x(CN_2)(CN_3)(C_2N_5)$. (b) A view of the $[C_2N_5]^{7-}$ units before chemical transformation. (c) A view of the C−N anions after chemical transformation at ambient conditions. (d) Schematic representation of the $[C_2N_5]^{7-}$ anion splitting into guanidinate $[CN_3]^{5-}$ and carbodiimide $[CN_2]^{2-}$ anions.

clearly observable in the spectrum. Nonstoichiometry in iron-containing compounds, where iron is present predominantly in the +II oxidation state with a smaller proportion in the +III state, is well-known, as exemplified by wüstite $Fe_{1-x}O$.[52,53]

Decompression of the DAC containing the sample demonstrated the recoverability of $Eu_4Fe_x(C_2N_5)_2$ down to ambient pressure (Tables S5 and S6). After ca. 1 day under ambient conditions, half of the $[C_2N_5]^{7-}$ anions split into guanidinate $[CN_3]^{5-}$ and carbodiimide $[CN_2]^{2-}$ anions (Figures 5b−d and S3), resulting in an abrupt increase of the unit cell volume and symmetry lowering (Table S6) in the compound, whose chemical formula can be written as $Eu_4Fe_x(CN_2)(CN_3)(C_2N_5)$.

The DFT+*U* optimized crystal structure of $Eu_4Fe(C_2N_5)_2$ (space group $P2_1/c$) at 50 GPa shows excellent agreement with the experimental crystal structure obtained from SCXRD (Tables S4 and S9). In the DFT calculations, we used an idealized chemical composition with $x = 1$ for both $Eu_4Fe_x(C_2N_5)_2$ and $Eu_4Fe_x(CN_2)(CN_3)(C_2N_5)$. At ambient pressure, the calculated unit cell volume of $Eu_4Fe(CN_2)(CN_3)(C_2N_5)$ differs from experiment by ∼5% with PBE+*U*, whereas PBEsol+*U* significantly improves the agreement with an error of less than 1.3% (Figure 2b, Table S9).

A BM3 fit to the pressure−volume data of $Eu_4Fe(C_2N_5)_2$ yields an equilibrium unit cell volume of 426 Å^3 and 406 Å^3 using PBE+*U* and PBEsol+*U*, respectively (Figure 2b, with an estimated bulk modulus in the range of 90−100 GPa). The lattice parameters calculated within PBE+*U* closely match the experiment at 50 GPa, whereas PBEsol+*U* provides better agreement at ambient pressure. At 50 GPa, $Eu_4Fe(C_2N_5)_2$ is dynamically stable as shown in Figure 6a. The experimental unit cell volumes at the intermediate pressure range 45−15 GPa fall between the PBE+*U* and PBEsol+*U* predictions (Figure 2b). Additionally, the lattice parameters (*a*, *b*, and *c*) of $Eu_4Fe(C_2N_5)_2$ show a smooth, monotonous decrease over the pressure range 10−50 GPa (Figure S5b). Below 10 GPa, lattice distortions emerge, indicating potential phase transformations from $Eu_4Fe(C_2N_5)_2$ to $Eu_4Fe(CN_2)(CN_3)(C_2N_5)$. This interpretation is further supported by phonon dispersion calculations for $Eu_4Fe(C_2N_5)_2$ at ambient pressure, which reveal imaginary phonon modes associated with Fe−N lattice vibrations, indicative of dynamic instability in $Eu_4Fe(C_2N_5)_2$ (Figure S9). Conversely, the $Eu_4Fe(CN_2)(CN_3)(C_2N_5)$ phase remains dynamically stable at ambient pressure (Figure 6b), supporting experimental observations.

Figure 6c shows the spin-polarized total and partial eDOS of $Eu_4Fe(C_2N_5)_2$ at 50 GPa, using the PBE+*U* functional. The phase exhibits an insulating behavior in both majority (spin-up) and minority (spin-down) spin channels, with energy gaps of 0.45 and 2.14 eV, respectively. The occupied Eu 4*f* states lie ∼ −6 eV below the Fermi level, while the unoccupied 4*f* states reside within the conduction band. Strong Fe 3*d* − N 2*p* hybridization occurs below the Fermi level for the spin-down channel, whereas in the spin-up channel the occupied Fe 3*d* states are distributed over a wider energy range of about 8 eV. The fundamental energy gap between the occupied (valence band) states and the unoccupied (conduction band) states is 0.45 eV, with unoccupied Eu 4*f* states exhibiting two distinct peaks, subject to a large exchange splitting induced by the localized moments of Eu 4*f* states with an energy width of 0.7

https://doi.org/10.1021/jacs.5c21756
J. Am. Chem. Soc. 2026, 148, 11915−11924

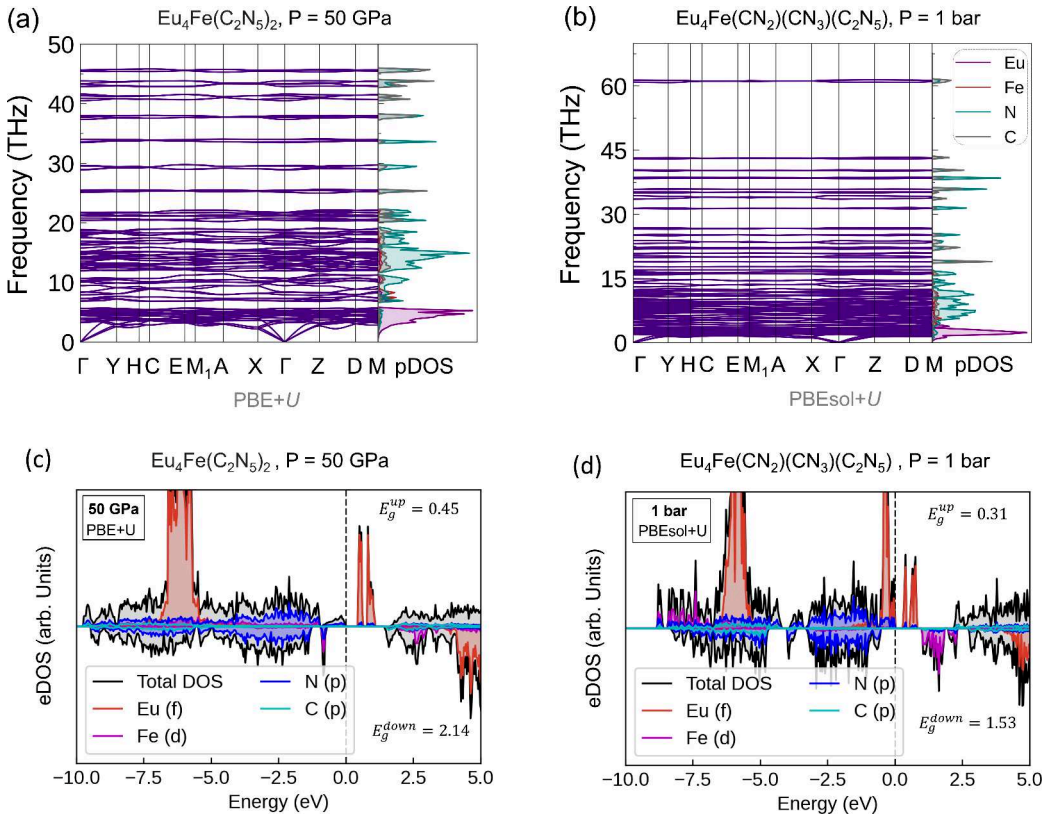

Figure 6. (a)−(b) Phonon dispersion relations and pDOS for $Eu_4Fe(C_2N_5)_2$ at 50 GPa and $Eu_4Fe(CN_2)(CN_3)(C_2N_5)$ at 1 bar using harmonic approximations. (c)−(d) Spin-resolved eDOS of $Eu_4Fe(C_2N_5)_2$ at 50 GPa and $Eu_4Fe(CN_2)(CN_3)(C_2N_5)$ at 1 bar calculated with the PBE+*U* and PBEsol+*U* functionals, respectively.

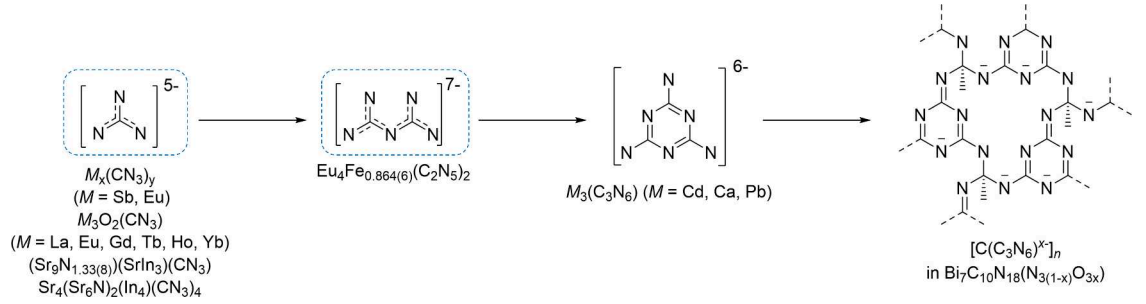

Figure 7. Schematic representation of the family of nitridocarbonates featuring progressive condensation of CN_3 building blocks: $[CN_3]^{5-}$,[12,31,32] $[C_2N_5]^{7-}$, $[C_3N_6]^{6-}$,[33,34] and $[C_4N_6^{x-}]_n$.[35]

eV. A more detailed analysis of the eDOS and magnetic ordering for $Eu_4Fe(C_2N_5)_2$ is provided in Supplementary Discussion S1.

Figure 6d shows the spin-polarized eDOS for $Eu_4Fe(CN_2)(CN_3)(C_2N_5)$ at 1 bar, using PBEsol+*U*. It exhibits a band gap of 0.31 eV for the spin-up channel and 1.53 eV for the spin-down channel. In $Eu_4Fe(CN_2)(CN_3)(C_2N_5)$, the occupied Eu 4*f* states appear at two distinct energy positions below the Fermi level: the majority of these states are positioned at −6 eV, while a smaller fraction appears just below the Fermi energy. A detailed analysis of the Wyckoff site resolved eDOS suggests that the Eu 4*f* states at −6 eV primarily originate from three europium sublattices (Eu1(2*a*), Eu2(2*a*), and Eu4(2*a*)), whereas the occupied states just below the Fermi level arise from a single Eu3(2*a*) sublattice (Figure S10d). This suggests a partial reduction of one Eu^{3+} ion to Eu^{2+} and oxidation of iron from +II to +III in $Eu_4Fe(CN_2)(CN_3)(C_2N_5)$.

CONCLUSIONS

High-pressure synthesis at 50(3) GPa enabled the stabilization of fully deprotonated guanidinate $[CN_3]^{5-}$ and pyronitridocarbonate $[C_2N_5]^{7-}$ anions in $Eu_5(CN_3)_3$ and $Eu_4Fe_x(C_2N_5)_2$ (x = 0.864(6)), respectively. The $[C_2N_5]^{7-}$ anion represents a key new member of the sp^2-hybridized C−N polyanion family, positioned between simple nitridocarbonates $[CN_3]^{5-}$ and melaminates $[C_3N_6]^{6-}$ (Figure 7). These results highlight the importance of precise pressure tuning and strategic selection of countercations for the design of highly charged nitridocarbonate species. While $[CN_3]^{5-}$ can be stabilized by the group 5 and group 15 cations (e.g., Sb as shown experimentally for $SbCN_3$,[31] or V, Nb, Ta as predicted for $(V,Nb,Ta)CN_3$[54]), stabilization of anions with the formal ionic charge of 7− is much more challenging and requires either a single element in a mixed-valence state, or a selected combination of two cations. In the case of $[C_2N_5]^{7-}$, such stabilization was achieved by a

https://doi.org/10.1021/jacs.5c21756
J. Am. Chem. Soc. 2026, 148, 11915−11924

combination of the Eu and Fe ions. This finding opens new directions for nitridocarbonate chemistry under extreme conditions.

Traditional high-pressure routes to *M*−C−N phases often rely on metal−nitrogen reactions with carbon provided by the diamond anvils or involve C−N precursors such as cyanuric triazide (C_3N_{12}).[31,32,35] Our approach employs precursors that already contain oxidized metals with fixed *M*:C and *M*:N ratios, offering more opportunities for stoichiometry control.

$Eu_4Fe_x(C_2N_5)_2$ significantly expands the chemistry of ternary and quaternary *M*−C−N compounds. Hitherto, only very few quaternary *RE*−Fe−C−N compounds had been explored, namely $RE_2Fe_{17}CN_x$ (*RE* = Y, Sm, Gd, Tb, Dy, and Er)[55] and $NdFe(CN)_6$.[56] The former compounds are interstitial carbonitrides, while the latter is a cyanide. Among ternary rare earth-containing nitridocarbonate compounds, only carbodiimides $RE_2(CN_2)_3$ (*RE* = Sc,[57] Sm,[58] Yb,[59] Lu[58,60]), carbodiimide nitrides $Ce_3(CN_2)_3N$,[61] cyanamides $EuCN_2$,[62] and dicyanamides $RE[N(CN)_2]_3$ (*RE* = La,[6] Ce,[6] Pr,[6] Nd,[6] Sm,[6] Eu,[6] and Gd[63]) are known to date.

Finally, decompression of $Eu_4Fe_x(C_2N_5)_2$ resulted in an interesting example of *in crystallo* chemistry: a single-crystal-to-single-crystal transformation in which 50% of the $[C_2N_5]^{7-}$ anions split into $[CN_2]^{2-}$ and $[CN_3]^{5-}$ anions while preserving the main structural motifs.

■ ASSOCIATED CONTENT

Supporting Information

The Supporting Information is available free of charge at https://pubs.acs.org/doi/10.1021/jacs.5c21756.

> Equations used in the statistical analysis of the C−N anions; crystallographic information; Synchrotron Mössbauer Source spectrum; supplementary DFT calculation results; supplementary discussion of theoretical computations (DOCX)

Accession Codes

Deposition Numbers 2495718−2495727 contain the supplementary crystallographic data for this paper. These data can be obtained free of charge via the joint Cambridge Crystallographic Data Centre (CCDC) and Fachinformationszentrum Karlsruhe Access Structures service.

■ AUTHOR INFORMATION

Corresponding Authors

Fariia Iasmin Akbar − *Institute of Inorganic and Analytical Chemistry, Goethe University Frankfurt, 60438 Frankfurt am Main, Germany;* orcid.org/0000-0002-6016-5849; Email: akbar@chemie.uni-frankfurt.de

Maxim Bykov − *Institute of Inorganic and Analytical Chemistry, Goethe University Frankfurt, 60438 Frankfurt am Main, Germany;* orcid.org/0000-0003-0248-1728; Email: maxim.bykov@chemie.uni-frankfurt.de

Nityasagar Jena − *Department of Physics, Chemistry and Biology (IFM), Linköping University, SE-58183 Linköping, Sweden;* orcid.org/0000-0002-4773-3848; Email: nityasagar.jena@liu.se

Authors

Christian Tobeck − *Institute of Inorganic and Materials Chemistry, University of Cologne, 50939 Cologne, Germany*

Pascal L. Jurzick − *Institute of Inorganic and Analytical Chemistry, Goethe University Frankfurt, 60438 Frankfurt am Main, Germany;* orcid.org/0009-0006-3044-3955

Niko T. Flosbach − *Institute of Inorganic and Materials Chemistry, University of Cologne, 50939 Cologne, Germany;* orcid.org/0000-0003-0778-762X

Valerio Cerantola − *Department of Earth and Environmental Sciences DISAT, University of Milano-Bicocca, I-20126 Milano, Italy;* orcid.org/0000-0002-2808-2963

Elena Bykova − *Institute of Geosciences, Goethe University Frankfurt, 60438 Frankfurt, Germany;* orcid.org/0000-0001-8652-024X

Lukas Brüning − *Institute of Inorganic and Analytical Chemistry, Goethe University Frankfurt, 60438 Frankfurt am Main, Germany;* orcid.org/0000-0002-3119-4464

Andrey Aslandukov − *Institute of Inorganic and Analytical Chemistry, Goethe University Frankfurt, 60438 Frankfurt am Main, Germany;* orcid.org/0000-0003-0988-6066

Dominik Spahr − *Institute of Geosciences, Goethe University Frankfurt, 60438 Frankfurt, Germany;* orcid.org/0000-0003-0489-5270

Valentin Kovalev − *Institute of Geosciences, Goethe University Frankfurt, 60438 Frankfurt, Germany;* orcid.org/0009-0000-0802-4179

Gaston Garbarino − *European Synchrotron Radiation Facility, 38043 Grenoble, France;* orcid.org/0000-0003-4780-9520

Anna Pakhomova − *European Synchrotron Radiation Facility, 38043 Grenoble, France;* orcid.org/0000-0003-4014-0203

Georgios Aprilis − *European Synchrotron Radiation Facility, 38043 Grenoble, France;* orcid.org/0000-0002-0020-9125

Nico Giordano − *Deutsches Elektronen-Synchrotron DESY, 22607 Hamburg, Germany;* orcid.org/0000-0001-9518-1251

Leonid Dubrovinsky − *Bavarian Research Institute of Experimental Geochemistry and Geophysics (BGI), University of Bayreuth, 95440 Bayreuth, Germany;* orcid.org/0000-0002-3717-7585

Mathias S. Wickleder − *Institute of Inorganic and Materials Chemistry, University of Cologne, 50939 Cologne, Germany;* orcid.org/0000-0002-8864-4227

Uwe Ruschewitz − *Institute of Inorganic and Materials Chemistry, University of Cologne, 50939 Cologne, Germany;* orcid.org/0000-0002-6511-6894

Igor A. Abrikosov − *Department of Physics, Chemistry and Biology (IFM), Linköping University, SE-58183 Linköping, Sweden;* orcid.org/0000-0001-7551-4717

Complete contact information is available at: https://pubs.acs.org/10.1021/jacs.5c21756

Author Contributions

The manuscript was written through contributions of all authors. All authors have given approval to the final version of the manuscript.

Funding

M.B. acknowledges the support of Deutsche Forschungsgemeinschaft (DFG Emmy-Noether project BY112/2−1). E.B. acknowledges the support of Deutsche Forschungsgemeinschaft (DFG Emmy-Noether project No. BY101/2−1). Co-funded by the European Union (ERC, HIPMAT, 101077963).

Views and opinions expressed are however those of the author(s) only and do not necessarily reflect those of the EU or the ERC. N.J. and I.A.A. acknowledge support by the Knut and Alice Wallenberg Foundation (Wallenberg Scholar grant no. KAW-2018.0194 and KAW-2023.0309). Support from the Swedish Research Council (VR) grant no. 2023−05358 and the Swedish Government Strategic Research Areas in Materials Science on Functional Materials at Linköping University (Faculty Grant SFO-Mat-LiU no. 2009 00971) is gratefully acknowledged. DFT calculations were enabled by high-performance computing (HPC) resources provided by the National Academic Infrastructure for Supercomputing in Sweden (NAISS) using Tetralith and Dardel at the National Supercomputer Center, Linköping University, partially funded by the Swedish Research Council through grant agreement no. 2022−06725. U.R. and C.T. acknowledge the support of Deutsche Forschungsgemeinschaft (project RU 546/15−1).

Notes

The authors declare no competing financial interest.

■ ACKNOWLEDGMENTS

We acknowledge DESY (Hamburg, Germany), a member of the Helmholtz Association HGF, for the provision of experimental facilities. Parts of this research were carried out at P02.2 (PETRAIII). We acknowledge the European Synchrotron Radiation Facility (ESRF) for provision of synchrotron radiation facilities under the proposal numbers CH-6885 (DOI: 10.15151/ESRF-ES-1685311408) and ES-1536 (DOI: 10.15151/ESRF-ES-1901553724).

■ REFERENCES

(1) Schulz, A.; Surkau, J. Main Group Cyanides: From Hydrogen Cyanide to Cyanido-Complexes. *Rev. Inorg. Chem.* **2023**, *43* (1), 49−188.

(2) Sougrati, M. T.; Darwiche, A.; Liu, X.; Mahmoud, A.; Hermann, R. P.; Jouen, S.; Monconduit, L.; Dronskowski, R.; Stievano, L. Transition-Metal Carbodiimides as Molecular Negative Electrode Materials for Lithium- and Sodium-Ion Batteries with Excellent Cycling Properties. *Angew. Chemie - Int. Ed.* **2016**, *55* (16), 5090−5095.

(3) Corkett, A. J.; Reckeweg, O.; Pöttgen, R.; Dronskowski, R. The $[NCN]^{2-}$ Carbodiimide Complex Anion and Its Compounds−A "Divalent Nitride" Unit for Nitridocarbonates in Materials and Applications. *Chem. Mater.* **2024**, *36* (19), 9107−9125.

(4) Jach, F.; Höhn, P.; Prots, Y.; Ruck, M. $Sr_4N[CN_2][C_2N]$: The First Carbodiimide Acetonitriletriide. *Eur. J. Inorg. Chem.* **2019**, *2019* (9), 1207−1211.

(5) Clark, W. P.; Köhn, A.; Niewa, R. The Quasi-Binary Acetonitriletriide $Sr_3[C_2N]_2$. *Angew. Chem., Int. Ed.* **2020**, *59* (1), 339−342.

(6) Jürgens, B.; Irran, E.; Schnick, W. Synthesis and Characterization of the Rare-Earth Dicyanamides $Ln[N(CN)_2]_3$ with *Ln*=La, Ce, Pr, Nd, Sm, and Eu. *J. Solid State Chem.* **2005**, *178* (1), 72−78.

(7) Bessler, K. E.; Gatto, C. C.; Romualdo, L. L.; Ellena, J. A.; Sales, M. J. de A. Pseudohalides of Main Group Metals: The Alcaline Earth Tricyanomethanides - The Crystal Structures of Calcium and Barium Tricyanomethanide. *Main Group Met. Chem.* **2007**, *30* (2−3), 135−142.

(8) Her, J.-H.; Stephens, P. W.; Davidson, R. A.; Min, K. S.; Bagnato, J. D.; van Schooten, K.; Boehme, C.; Miller, J. S. Weak Ferromagnetic Ordering of the $Li^+[TCNE]^{\bullet-}$ (TCNE = Tetracyanoethylene) Organic Magnet with an Interpenetrating Diamondoid Structure. *J. Am. Chem. Soc.* **2013**, *135* (48), 18060−18063.

(9) Webster, O. W. Cyanocarbons: A Classic Example of Discovery-driven Research. *J. Polym. Sci. A Polym. Chem.* **2002**, *40* (2), 210−221.

(10) Hipps, K. W.; Geiser, U.; Mazur, U.; Willett, R. D. Cesium Pentacyanopropenide. Crystal Structure, Vibrational Spectra and Assignments, and Vibronic Structure in the Visible Emission Spectrum. *J. Phys. Chem.* **1984**, *88* (12), 2498−2504.

(11) Jäger, L.; Wagner, C.; Hanke, W. Crystal and Molecular Structure of Silver(1,1,2,3,3-Pentacyanopropenide). *J. Mol. Struct.* **2000**, *525* (1−3), 107−111.

(12) Stelzer, R. U.; Wang, Y.; Dronskowski, R.; Niewa, R. $(Sr_9N_{1.33(8)})(SrIn_3)[CN_3]$ and $Sr_4(Sr_6N)_2[In_4][CN_3]_4$: Two Fully Deprotonated Guanidinates Accessible from Pressureless Sodium Flux Synthesis. *Inorg. Chem.* **2025**, *64* (14), 6845−6856.

(13) Irran, E.; Jürgens, B.; Schnick, W. Trimerization of Alkali Dicyanamides $M[N(CN)_2]$ and Formation of Tricyanomelaminates $M_3[C_6N_9]$ (M = K, Rb) in the Melt: Crystal Structure Determination of Three Polymorphs of $K[N(CN)_2]$, Two of $Rb[N(CN)_2]$, and One of $K_3[C_6N_9]$ and $Rb_3[C_6N_9]$ from X-ray Powder Diffractometry. *Chem. Eur. J.* **2001**, *7* (24), 5372−5381.

(14) Horvath-Bordon, E.; Kroke, E.; Svoboda, I.; Fuess, H.; Riedel, R. Potassium Melonate, $K_3[C_6N_7(NCN)_3]\cdot 5H_2O$, and Its Potential Use for the Synthesis of Graphite-like C_3N_4 Materials. *New J. Chem.* **2005**, *29* (5), 693−699.

(15) Joalland, B.; Jamal-Eddine, N.; Kłos, J.; Lique, F.; Trolez, Y.; Guillemin, J.-C.; Carles, S.; Biennier, L. Low-Temperature Reactivity of $C_{2n+1}N^-$ Anions with Polar Molecules. *J. Phys. Chem. Lett.* **2016**, *7* (15), 2957−2961.

(16) Khairallah, G.; Peel, J. B. Cyano Adduct-Anions of [60]-Fullerene Observed by Electrospray Mass Spectrometry. *Chem. Commun.* **1997**, *60* (3), 253−254.

(17) Khairallah, G.; Peel, J. B. Identification of Cyano Dianions of C_{60} by Electrospray Mass Spectrometry. *Chem. Phys. Lett.* **1997**, *268* (3−4), 218−222.

(18) Khairallah, G.; Peel, J. B. Cyano Adduct Anions of C_{70}: Electrospray Mass Spectrometric Studies. *J. Phys. Chem. A* **1997**, *101* (36), 6770−6774.

(19) Klapötke, T. M.; Stierstorfer, J. The CN_7^- Anion. *J. Am. Chem. Soc.* **2009**, *131* (3), 1122−1134.

(20) Meng, Y. Poly[μ-(5,5′-Diazenediylditetrazolido)-Dicaesium]. *Acta Crystallogr.* **2011**, *E67*, No. m453.

(21) Laus, G.; Kahlenberg, V.; Wurst, K.; Schottenberger, H.; Fischer, N.; Stierstorfer, J.; Klapötke, T. M. Synthesis and Crystal Structures of New 5,5′-Azotetrazolates. *Crystals* **2012**, *2* (1), 127−136.

(22) Luo, L.; Hao, W.; Jin, B.; Guo, Z.; Guo, J.; Liu, Q.; Deng, H.; Peng, R. Solvent-Free 3D Layered Energetic Metal Organic Framework: Structure, Stability, and Its Laser Response. *J. Solid State Chem.* **2023**, *317*, No. 123607.

(23) Laniel, D.; Winkler, B.; Koemets, E.; Fedotenko, T.; Bykov, M.; Bykova, E.; Dubrovinsky, L.; Dubrovinskaia, N. Synthesis of Magnesium-Nitrogen Salts of Polynitrogen Anions. *Nat. Commun.* **2019**, *10*, 4515.

(24) Laniel, D.; Weck, G.; Gaiffe, G.; Garbarino, G.; Loubeyre, P. High-Pressure Synthesized Lithium Pentazolate Compound Metastable under Ambient Conditions. *J. Phys. Chem. Lett.* **2018**, *9* (7), 1600−1604.

(25) Steele, B. A.; Stavrou, E.; Crowhurst, J. C.; Zaug, J. M.; Prakapenka, V. B.; Oleynik, I. I. High-Pressure Synthesis of a Pentazolate Salt. *Chem. Mater.* **2017**, *29* (2), 735−741.

(26) Laniel, D.; Trybel, F.; Yin, Y.; Fedotenko, T.; Khandarkhaeva, S.; Aslandukov, A.; Aprilis, G.; Abrikosov, A. I.; Bin Masood, T.; Giacobbe, C.; Bright, E. L.; Glazyrin, K.; Hanfland, M.; Wright, J.; Hotz, I.; Abrikosov, I. A.; Dubrovinsky, L.; Dubrovinskaia, N. Aromatic Hexazine $[N_6]^{4-}$ Anion Featured in the Complex Structure of the High-Pressure Potassium Nitrogen Compound K_9N_{56}. *Nat. Chem.* **2023**, *15* (5), 641−646.

(27) Wang, Y.; Bykov, M.; Chepkasov, I.; Samtsevich, A.; Bykova, E.; Zhang, X.; Jiang, S.; Greenberg, E.; Chariton, S.; Prakapenka, V. B.; Oganov, A. R.; Goncharov, A. F. Stabilization of Hexazine Rings in Potassium Polynitride at High Pressure. *Nat. Chem.* **2022**, *14* (7), 794−800.

(28) Aslandukov, A.; Trybel, F.; Aslandukova, A.; Laniel, D.; Fedotenko, T.; Khandarkhaeva, S.; Aprilis, G.; Giacobbe, C.; Lawrence Bright, E.; Abrikosov, I. A.; Dubrovinsky, L.; Dubrovinskaia, N. Anionic N_{18} Macrocycles and a Polynitrogen Double Helix in Novel Yttrium Polynitrides YN_6 and Y_2N_{11} at 100 GPa. *Angew. Chem., Int. Ed.* **2022**, *61* (34), e202207469.
(29) Laniel, D.; Winkler, B.; Fedotenko, T.; Pakhomova, A.; Chariton, S.; Milman, V.; Prakapenka, V.; Dubrovinsky, L.; Dubrovinskaia, N. High-Pressure Polymeric Nitrogen Allotrope with the Black Phosphorus Structure. *Phys. Rev. Lett.* **2020**, *124* (21), No. 216001.
(30) Aslandukov, A.; Aslandukova, A.; Laniel, D.; Khandarkhaeva, S.; Yin, Y.; Akbar, F. I.; Chariton, S.; Prakapenka, V.; Bright, E. L.; Giacobbe, C.; Wright, J.; Comboni, D.; Hanfland, M.; Dubrovinskaia, N.; Dubrovinsky, L.; Han, M.; Dubrovinskaia, N.; Dubrovinsky, L. Stabilization of N_6 and N_8 Anionic Units and 2D Polynitrogen Layers in High-Pressure Scandium Polynitrides. *Nat. Commun.* **2024**, *15* (1), 2244.
(31) Brüning, L.; Jena, N.; Bykova, E.; Jurzick, P. L.; Flosbach, N. T.; Mezouar, M.; Hanfland, M.; Giordano, N.; Fedotenko, T.; Winkler, B.; Abrikosov, I. A.; Bykov, M. Stabilization of Guanidinate Anions $[CN_3]^{5-}$ in Calcite-Type $SbCN_3$. *Angew. Chem., Int. Ed.* **2023**, *62*, e202311519 DOI: 10.1002/anie.202311519.
(32) Aslandukov, A.; Jurzick, P. L.; Bykov, M.; Aslandukova, A.; Chanyshev, A.; Laniel, D.; Yin, Y.; Akbar, F. I.; Khandarkhaeva, S.; Fedotenko, T.; Glazyrin, K.; Chariton, S.; Prakapenka, V.; Wilhelm, F.; Rogalev, A.; Comboni, D.; Hanfland, M.; Dubrovinskaia, N.; Dubrovinsky, L. Stabilization Of The CN_3^{5-} Anion In Recoverable High-pressure $Ln_3O_2(CN_3)$ (Ln = La, Eu, Gd, Tb, Ho, Yb) Oxoguanidinates. *Angew. Chem., Int. Ed.* **2023**, *62* (47), e202311516.
(33) Ranieri, U.; Liang, A.; Lamb, C.; Spender, J.; Bolton, S.; Aslandukov, A.; Massani, B.; Tasnádi, F.; Autran, P.-O.; Ball, J. A. D.; Rosa, A. D.; Wang, B.; Trybel, F.; Laniel, D. High-Pressure Synthesis of Two $Pb_3(C_3N_6)$ Polymorphs Featuring Fully Deprotonated $[C_3N_6]^{6-}$ Melaminate Anions. *J. Am. Chem. Soc.* **2025**, *147* (39), 35431−35437.
(34) Jurzick, P. L.; Brüning, L.; Winkler, B.; Wang, Y.; Dronskowski, R.; Bykova, E.; Spahr, D.; Hanfland, M.; Wehinger, B.; Giordano, N.; Bykov, M. Stabilization of Fully Deprotonated Melaminate Anions $(C_3N_6)^{6-}$ in $M_3(C_3N_6)$ (M = Cd, Ca). *J. Am. Chem. Soc.* **2026**, *148*, 2843.
(35) Brüning, L.; Jena, N.; Jurzick, P. L.; Bykova, E.; Giordano, N.; Mezouar, M.; Abrikosov, I. A.; Bykov, M. High-Pressure Synthesis of Crystalline Double-Layer Carbon Nitride Networks Stabilized in $Bi_7C_{10}N_{18}(N_{3(1-x)}O_{3x})$. *Angew. Chem., Int. Ed.* **2025**, *64*, e202506406 DOI: 10.1002/anie.202506406.
(36) Aslandukov, A.; Liang, A.; Ehn, A.; Trybel, F.; Yin, Y.; Aslandukova, A.; Akbar, F. I.; Ranieri, U.; Spender, J.; Howie, R. T.; Bright, E. L.; Wright, J.; Hanfland, M.; Garbarino, G.; Mezouar, M.; Fedotenko, T.; Abrikosov, I. A.; Dubrovinskaia, N.; Dubrovinsky, L.; Laniel, D. Synthesis of $LaCN_3$, $TbCN_3$, $CeCN_5$, and $TbCN_5$ Polycarbonitrides at Megabar Pressures. *J. Am. Chem. Soc.* **2024**, *146* (26), 18161−18171.
(37) Spahr, D.; Bayarjargal, L.; Bykov, M.; Brüning, L.; Jurzick, P. L.; Wang, Y.; Milman, V.; Refson, K.; Mezouar, M.; Winkler, B. $Ca_3[C_2O_5]_2[CO_3]$ Is a Pyrocarbonate Which Can Be Formed at *p*, *T*-Conditions Prevalent in the Earth's Transition Zone. *Commun. Chem.* **2024**, *7* (1), 238.
(38) Spahr, D.; Bayarjargal, L.; Bykov, M.; Brüning, L.; Reuter, T. H.; Milman, V.; Liermann, H.-P.; Winkler, B. High-Pressure Synthesis of Acentric Sodium Pyrocarbonate, $Na_2[C_2O_5]$. *Dalton Trans.* **2024**, *53* (1), 40−44.
(39) Spahr, D.; Bayarjargal, L.; Haussühl, E.; Luchitskaia, R.; Friedrich, A.; Milman, V.; Fedotenko, T.; Winkler, B. Twisted $[C_2O_5]^{2-}$-Groups in $Ba[C_2O_5]$ Pyrocarbonate. *Chem. Commun.* **2023**, *59* (80), 11951−11954.
(40) Spahr, D.; König, J.; Bayarjargal, L.; Luchitskaia, R.; Milman, V.; Perlov, A.; Liermann, H.-P.; Winkler, B. Synthesis and Structure of $Pb[C_2O_5]$: An Inorganic Pyrocarbonate Salt. *Inorg. Chem.* **2022**, *61* (26), 9855−9859.
(41) Spahr, D.; König, J.; Bayarjargal, L.; Milman, V.; Perlov, A.; Liermann, H.-P.; Winkler, B. $Sr[C_2O_5]$ Is an Inorganic Pyrocarbonate Salt with $[C_2O_5]^{2-}$ Complex Anions. *J. Am. Chem. Soc.* **2022**, *144* (7), 2899−2904.
(42) Spahr, D.; Bayarjargal, L.; Bykov, M.; Brüning, L.; Jurzick, P. L.; Milman, V.; Giordano, N.; Mezouar, M.; Winkler, B. Synthesis and Characterization of Lithium Pyrocarbonate ($Li_2[C_2O_5]$) and Lithium Hydrogen Pyrocarbonate ($Li[HC_2O_5]$). *Angew. Chem., Int. Ed.* **2024**, *63* (49), No. e202409822.
(43) Bertschler, E.; Bräuniger, T.; Dietrich, C.; Janek, J.; Schnick, W. $Li_{47}B_3P_{14}N_{42}$—A Lithium Nitridoborophosphate with $[P_3N_9]^{12-}$, $[P_4N_{10}]^{10-}$, and the Unprecedented $[B_3P_3N_{13}]^{15-}$ Ion. *Angew. Chem., Int. Ed.* **2017**, *56* (17), 4806−4809.
(44) Akbar, F. I.; Aslandukova, A.; Aslandukov, A.; Yin, Y.; Trybel, F.; Khandarkhaeva, S.; Fedotenko, T.; Laniel, D.; Bykov, M.; Bykova, E.; Dubrovinskaia, N.; Dubrovinsky, L. High-Pressure Synthesis of Dysprosium Carbides. *Front. Chem.* **2023**, *11*, 1210081.
(45) Akbar, F. I.; Aslandukova, A.; Yin, Y.; Aslandukov, A.; Laniel, D.; Bykova, E.; Bykov, M.; Bright, E. L.; Wright, J.; Comboni, D.; Hanfland, M.; Dubrovinskaia, N.; Dubrovinsky, L. High-Pressure Dysprosium Carbides Containing Carbon Dimers, Trimers, Chains, and Ribbons. *Carbon* **2024**, *228*, No. 119374.
(46) Bharatam, P. V.; Patel, D. S.; Iqbal, P. Pharmacophoric Features of Biguanide Derivatives: An Electronic and Structural Analysis. *J. Med. Chem.* **2005**, *48* (24), 7615−7622.
(47) Raczyńska, E. D.; Hallman, M.; Kolczyńska, K.; Stępniewski, T. M. On the Harmonic Oscillator Model of Electron Delocalization (HOMED) Index and Its Application to Heteroatomic π-Electron Systems. *Symmetry* **2010**, *2* (3), 1485−1509.
(48) Sørensen, G. O.; Mahler, L.; Rastrup-Andersen, N. Microwave Spectra of [^{15}N] and [^{13}C] Pyridines, Quadrupole Coupling Constants, Dipole Moment and Molecular Structure of Pyridine. *J. Mol. Struct.* **1974**, *20* (1), 119−126.
(49) Eichhorn, K. Bond-Length−Bond-Strength Correlation between N−O and C−N of Pyridine N-Oxides. *Acta Crystallogr.* **1987**, *B43*, 111−112.
(50) Cerantola, V.; McCammon, C.; Kupenko, I.; Kantor, I.; Marini, C.; Wilke, M.; Ismailova, L.; Solopova, N.; Chumakov, A.; Pascarelli, S.; Dubrovinsky, L. High-Pressure Spectroscopic Study of Siderite ($FeCO_3$) with a Focus on Spin Crossover. *Am. Mineral.* **2015**, *100* (11−12), 2670−2681.
(51) Gütlich, P.; Bill, E.; Trautwein, A. X. *Mössbauer Spectroscopy and Transition Metal Chemistry*; Springer Berlin, Heidelberg, 2011. DOI: 10.1007/978-3-540-88428-6.
(52) Gavarri, J.-R.; Carel, C. The Complex Nonstoichiometry of Wüstite $Fe_{1-z}O$: Review and Comments. *Prog. Solid State Chem.* **2019**, *53*, 27−49.
(53) Liang, Z.; Li, K.; Zhang, J.; Conejo, A. N. Insights into Defect Cluster Formation in Non-Stoichiometric Wustite ($Fe_{1-x}O$) at Elevated Temperatures: Accurate Force Field from Deep Learning. *npj Comput. Mater.* **2025**, *11* (1), 32.
(54) Luo, D.; Qiao, X.; Dronskowski, R. Predicting Nitrogen-Based Families of Compounds: Transition-Metal Guanidinates TCN_3 (T = V, Nb, Ta) and Ortho-Nitrido Carbonates T'_2CN_4 (T′=Ti, Zr, Hf). *Angew. Chem., Int. Ed.* **2021**, *60* (1), 486−492.
(55) Yang, Y.; Pan, Q.; Zhang, X.; Ge, S. Magnetic Properties of $R_2Fe_{17}CN_X$. *J. Appl. Phys.* **1992**, *72* (7), 2989−2992.
(56) Jiao, Y.; Gao, Q.; Sanson, A.; Liang, E.; Sun, Q.; Chen, J. Understanding Large Negative Thermal Expansion of $NdFe(CN)_6$ through the Electronic Structure and Lattice Dynamics. *Inorg. Chem.* **2022**, *61* (20), 7813−7819.
(57) Kallenbach, P.; Ströbele, M.; Meyer, H. Missing Carbodiimide and Oxide Carbodiimide of Scandium: $Sc_2(CN_2)_3$ and $Sc_2O_2(CN_2)$. *Z. Anorg. Allg. Chem.* **2020**, *646* (15), 1281−1284.
(58) Neukirch, M.; Tragl, S.; Meyer, H.-J. Syntheses and Structural Properties of Rare Earth Carbodiimides. *Inorg. Chem.* **2006**, *45* (20), 8188−8193.

(59) Reckeweg, O.; Schleid, T.; DiSalvo, F. J. Synthesis, Crystal Structure and Optical Spectra of $Yb_2[CN_2]_3$. *Z. Naturforsch.* **2007**, *62b* (5), 658−662.
(60) Glaser, J.; Unverfehrt, L.; Bettentrup, H.; Heymann, G.; Huppertz, H.; Jüstel, T.; Meyer, H.-J. Crystal Structures, Phase-Transition, and Photoluminescence of Rare Earth Carbodiimides. *Inorg. Chem.* **2008**, *47* (22), 10455−10460.
(61) Unverfehrt, L.; Ströbele, M.; Glaser, J.; Meyer, H.-J. The Many Faces of Rare Earth Carbodiimide Compounds. *Z. Anorg. Allg. Chem.* **2009**, *635* (12), 1947−1952.
(62) Reckeweg, O.; DiSalvo, F. J. $EuCN_2$ — The First, but Not Quite Unexpected Ternary Rare Earth Metal Cyanamide. *Z. Anorg. Allg. Chem.* **2003**, *629* (2), 177−179.
(63) Nag, A.; Schnick, W. Synthesis, Crystal Structure and Thermal Behavior of Gadolinium Dicyanamide Dihydrate $Gd[N(CN)_2]_3 \cdot 2H_2O$. *Z. Anorg. Allg. Chem.* **2006**, *632* (4), 609−614.

https://doi.org/10.1021/jacs.5c21756
J. Am. Chem. Soc. 2026, 148, 11915−11924